Global energy conversion rate from geostrophic flows into internal lee waves in the deep ocean

Maxim Nikurashin[1] and Raffaele Ferrari[2]

[1] A global estimate of the energy conversion rate from geostrophic flows into internal lee waves in the ocean is presented. The estimate is based on a linear theory applied to bottom topography at O(1–10) km scales obtained from single beam echo soundings, to bottom stratification estimated from climatology, and to bottom velocity obtained from a global ocean model. The total energy flux into internal lee waves is estimated to be 0.2 TW which is 20% of the global wind power input into the ocean. The geographical distribution of the energy flux is largest in the Southern Ocean which accounts for half of the total energy flux. The results suggest that the generation of internal lee waves at rough topography is a significant energy sink for the geostrophic flows as well as an important energy source for internal waves and the associated turbulent mixing in the deep ocean. **Citation:** Nikurashin, M., and R. Ferrari (2011), Global energy conversion rate from geostrophic flows into internal lee waves in the deep ocean, *Geophys. Res. Lett.*, *38*, L08610, doi:10.1029/2011GL046576.

1. Introduction

[2] The wind power input into geostrophic flows in the ocean is estimated to be of $O(1)$ TW (1 TW = 10^{12} W) and is dominated by the work done in the Southern Ocean (SO) [*Wunsch*, 1998]. This wind power input drives all the major ocean currents such as the western boundary currents in mid-latitudes, the equatorial current system, and the Antarctic Circumpolar Current (ACC) in the SO. This energy is subsequently converted, through baroclinic instability, into a vigorous geostrophic eddy field. It is believed that the eddy field in turn loses its energy through friction in bottom boundary layers [*Arbic and Flierl*, 2004] and along western boundaries [*Zhai et al.*, 2010], and through internal wave generation at rough topography [*Nikurashin and Ferrari*, 2010a]. *Sen et al.* [2008] estimate that 0.2–0.8 TW of the wind power input into geostrophic flows dissipates in the bottom boundary layer by quadratic bottom drag. *Zhai et al.* [2010] speculate that western boundaries act as a 'graveyard' for the westward-propagating ocean eddies dissipating 0.1–0.3 TW in mid-latitudes. The fraction of the wind energy input converted into internal waves at rough topography remains unknown.

[3] Indirect evidence for generation of internal waves by geostrophic flows has emerged in the SO. Turbulent energy dissipation estimates show that mixing is greatly enhanced within O(1) km above rough topography and is correlated with the magnitude of the bottom geostrophic flow [e.g., *Kunze et al.*, 2006]. The observed mixing appears to be sustained by internal waves generated by the bottom currents flowing over small-scale topographic features. Using idealized numerical simulations and linear theory, *Nikurashin and Ferrari* [2010a, hereafter NF10a] showed that geostrophic flows over small-scale topography in typical oceanographic conditions can drive substantial mixing in the bottom kilometer at rates consistent with observations and that linear lee wave theory gives a good prediction of the energy conversion rate at sub-critical and critical topography. *Nikurashin and Ferrari* [2010b, hereafter NF10b] applied the linear lee wave theory to single beam and multibeam soundings and LADCP velocity data in the southeast Pacific and Drake Passage (DP) regions of the SO and showed that the energy flux into lee waves and the associated wave breaking and mixing in the two regions is of the same order of magnitude as the energy dissipation inferred from observations.

[4] In the present study, the analysis presented by NF10b is extended to a global estimate of the energy conversion rate from geostrophic flows into internal lee waves. The energy conversion rate is computed by applying a linear theory of lee wave generation to topographic spectra estimated from single beam soundings, to bottom stratification estimated from climatology, and to bottom geostrophic flows obtained from a global ocean model. The theory is briefly summarized below, but the reader is referred to NF10a and NF10b for a more detailed presentation.

2. Method

[5] Internal lee waves are generated in a stratified fluid when a quasi-steady current flows over small-scale topographic features. Linear theory [*Bell*, 1975] shows that, in the limit of subcritical topography, i.e., when the topographic slope is smaller than the internal wave slope, the energy flux E radiated in lee waves is given by,

$$E = \frac{\rho_0}{4\pi^2} \int_{-\infty}^{+\infty} \int_{-\infty}^{+\infty} P(k,l) \frac{(\mathbf{U} \cdot \mathbf{k})}{|\mathbf{k}|} \sqrt{N^2 - (\mathbf{U} \cdot \mathbf{k})^2}$$
$$\cdot \sqrt{(\mathbf{U} \cdot \mathbf{k})^2 - f^2} \ dkdl, \tag{1}$$

where $\mathbf{k} = (k, l)$ is the wavenumber vector, $P(k, l)$ the two-dimensional topographic spectrum, $\mathbf{U}$ the bottom velocity vector, f the Coriolis frequency, N is the bottom stratification, and ρ_0 a reference density. Linear theory predicts that the energy flux at each wavenumber depends on the mag-

---
[1]Program in Atmospheric and Oceanic Sciences, Princeton University, Princeton, New Jersey, USA.
[2]Department of Earth, Atmospheric and Planetary Sciences, Massachusetts Institute of Technology, Cambridge, Massachusetts, USA.

nitude of the topographic spectrum and the relative orientation of the velocity and wavenumber vectors. Without loss of generality, the reference frame can be rotated to have the 'k'-axis along the velocity vector $\mathbf{U}$ at each location and the expression for E reduces to,

$$E = \frac{\rho_0|\mathbf{U}|}{2\pi} \int_{|f|/|\mathbf{U}|}^{N/|\mathbf{U}|} P_*(k)\sqrt{N^2 - |\mathbf{U}|^2 k^2}\sqrt{|\mathbf{U}|^2 k^2 - f^2}\,dk, \quad (2)$$

where $\mathbf{k} = (k, l)$ is now the wavenumber in the reference frame along and across the mean flow $\mathbf{U}$ and

$$P_*(k) = \frac{1}{2\pi}\int_{-\infty}^{+\infty} \frac{|k|}{|\mathbf{k}|}P(k,l)\,dl \quad (3)$$

is the effective topographic spectrum. The wave radiation from two-dimensional topography reduces to an equivalent one-dimensional problem in the direction along the mean flow with the topography spectrum given by $P_*(k)$.

[6] Simulations with monochromatic topography by NF10a show that the characteristics of lee wave radiation are controlled by the steepness parameter, $\epsilon = Nh_0/|\mathbf{U}|$, where h_0 is the amplitude of the monochromatic topography. The energy flux increases quadratically with ϵ as predicted by linear theory for $\epsilon \leq \epsilon_c$, where $\epsilon_c = 0.7$ is a critical steepness parameter. For $\epsilon > \epsilon_c$ some fraction of the flow becomes blocked by topography and the energy flux saturates and ceases to increase with ϵ. To characterize the criticality of topography to lee wave radiation globally, the steepness parameter is generalized for a multichromatic topography as $\epsilon = N\sqrt{2}h_{rms}/|\mathbf{U}|$, where h_{rms} is the rms height of topography in the radiative wavenumber range. This definition is rather crude, but it captures the nonlinearity of the mean flow-topography interaction for the multichromatic topographic simulations described by NF10b and it reduces to a definition used by NF10a for monochromatic topography. To account for the suppression of the energy conversion at super-critical topography, the expression (2) is multiplied by $(\epsilon_c/\epsilon)^2$ at all locations whenever $\epsilon > \epsilon_c$.

3. Data

[7] The energy conversion rate is estimated by evaluating the integral in (2) over the range of radiative wavenumbers at each geographic location. The data needed to make an estimate are the topographic spectrum, bottom stratification, and bottom velocity.

3.1. Topographic Spectra

[8] Linear theory predicts that lee waves radiate from topographic features with wavenumbers k in the range $f/|\mathbf{U}| < k < N/|\mathbf{U}|$, which spans wavelengths from O(100) m to O(10) km for typical oceanic parameters ($N = 10^{-2}$ s^{-1} and $|\mathbf{U}| = 1$–10 cm s^{-1}). Topographic features with scales shorter than 10–20 km are not resolved by satellite bathymetry and are only available from single beam or multibeam soundings.

[9] Multibeam soundings generate two dimensional maps of topography at a resolution of 200–500 m and would be the dataset of choice for computing lee wave radiation.

Unfortunately multibeam soundings come in 5–20 km wide swaths of seafloor over few regions in the ocean and cannot be used for global calculations. A global prediction of abyssal hill roughness statistics was generated by *Goff and Arbic* [2010]. However this prediction is based on empirical relationships between topographic features and tectonic processes. Alternatively we opted to use single beam soundings which provide in-situ one-dimensional topographic sections.

[10] A somewhat coarse resolution and the inability to characterize two dimensional anisotropies in topographic hills are the major limitations of the single beam soundings. Both issues, however, do not severely affect the estimate presented in this study. Although lee waves can be radiated from scales as small as 100 m, we show below that the global energy conversion rate is dominated by waves radiated from scales larger than O(1) km. *Becker and Sandwell* [2008] compared single beam and multibeam soundings and concluded that the single beam soundings adequately characterize topography down to O(1) km scales. The lack of anisotropy information is also of little consequence for present purposes. The geostrophic velocity field is dominated by transient eddies, whose velocity direction can span the whole 360° over a few eddy turnover times. Hence the time-mean radiation is an average over geostrophic flows impinging on rough topography at all possible angles with respect to its anisotropy. Ship tracks are randomly oriented with respect to the topographic anisotropy [*Becker and Sandwell*, 2008] and provide a good characterization of topographic roughness in all possible directions as long as one averages over multiple tracks.

[11] The energy radiation calculation requires an estimate of the effective topographic spectrum in (3). This spectrum is obtained by least-square fitting one dimensional spectra from single beam tracks to the theoretical spectrum derived by *Goff and Jordan* [1988]. *Goff and Jordan* [1988] proposed a parametric representation of the topographic spectrum at O(0.1–100) km scales based on a statistical description of abyssal hills formed by ridge-crest processes, off-ridge tectonics, and volcanism,

$$P_{GJ}(k,l) = \frac{2\pi h^2(\mu-2)}{k_0 l_0}\left(1 + \frac{k^2}{k_0^2} + \frac{l^2}{l_0^2}\right)^{-\mu/2}. \quad (4)$$

The model spectrum is flat at scales larger than the inverse of the roll-off wavenumbers k_0 and l_0, i.e., scales of O(10–100) km, where abyssal hills transition into large scale topographic features, and rolls-off anisotropically at smaller scales with a slope $\mu/2$. Assuming that topography is isotropic, i.e., $\kappa_0 = k_0 = l_0$, and that lee waves are radiated from topographic scales such that $|\mathbf{k}|^2 \gg \kappa_0^2$, a one-dimensional form of the model spectrum (sampled by single beam soundings) can be obtained by integration of the two-dimensional spectrum along the wavenumber component l,

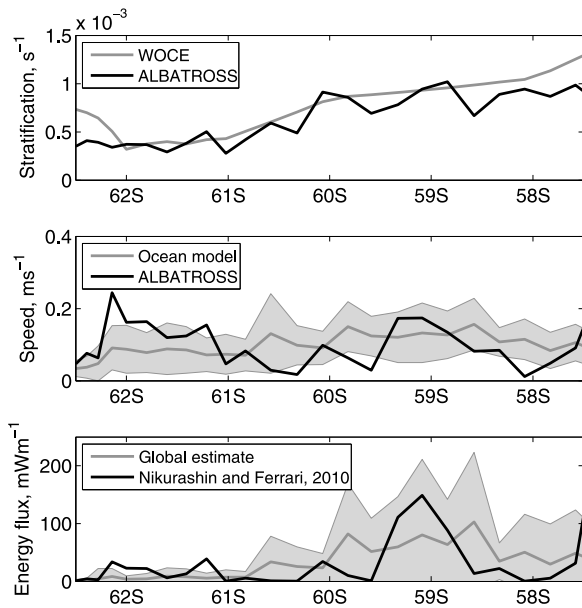$$P_{1d}(k) = \frac{1}{2\pi}\int_{-\infty}^{+\infty} P_{GJ}(k,l)\,dl \simeq P_0 k^{-\mu+1}, \quad (5)$$

Figure 1. (top) Bottom stratification across DP estimated from (gray) the WOCE hydrographic atlas and (black) the ALBATROSS data; (middle) (gray) The mean and standard deviation of the bottom speed in (m s^{-1}) from the GFDL isopycnal ocean model, (black) the bottom speed in (m s^{-1}) from the ALBATROSS data; (bottom)(gray) The mean and standard deviation of the energy conversion into lee waves in (mW m^{-2}) across DP from a global estimate and (black) from the ALBATROSS data.

where P_0 is the spectral level given in terms of parameters of the two-dimensional spectrum. NF10b show that the effective topographic spectrum in (3) is related to $P_{1d}(k)$ as

$$P_*(k) = P_{1d}(k)\frac{B[1/2, (\mu - 1)/2]}{B[1/2, \mu/2]}, \qquad (6)$$

where B is the beta function.

[12] Spectral characteristics of topography at O(1–10) km scales are estimated using single beam soundings from the U.S. National Geophysical Data Center. The single beam soundings were collected during marine cruises from 1953 to the present and have a worldwide coverage, even though the density of tracks in the Northern Hemisphere is higher than in the Southern Hemisphere. Along-track resolution varies among tracks from a few hundred meters to a few kilometers. The data, as well as their detailed description, can be found at http://www.ngdc.noaa.gov/mgg/geodas/trackline.html. *Becker and Sandwell* [2008] discuss the removal of blunders and outliers.

[13] Single beam soundings are analyzed as follows. All soundings from waters deeper than 500 m and with along-track resolution of at least 2 km are divided into 50 km long segments. The total number of ~200,000 segments is used. For each segment a large-scale topographic slope is removed by fitting a straight line, before the along-track topographic spectrum is computed. Spectra are binned and averaged over a 3° × 3° grid. Parameters P_0 and μ of the one-dimensional

model spectrum in (5) are estimated for each grid cell by fitting the model spectrum in (5) to the spectrum estimated from data in a least square sense in the 2 to 20 km wavelength range. Values in grid cells where topographic data are absent are estimated from neighboring cells by interpolation.

3.2. Bottom Stratification

[14] The bottom stratification is computed using the WOCE hydrographic atlas [*Gouretski and Koltermann*, 2004] as $N^2 = -g/\rho_0 \partial\rho/\partial z$, where g is gravity, ρ_0 is a reference density, and ρ is the potential density locally referenced. The vertical gradient of potential density is evaluated from the bottom two potential density values, spanning the bottom 500 m, using finite-differences.

3.3. Bottom Velocity

[15] The bottom velocity is taken from an isopycnal ocean model developed at GFDL and configured for global simulations with 49 layers and a 1/8° Mercator resolution [*Adcroft et al.*, 2010]. The bottom velocity is defined as the velocity from the deepest isopycnal layer whose thickness varies from 200 to 500 m over mid-ocean ridges and up to ~1 km over deep abyssal plains. The lack of model resolution within the bottom 20–40% of the water column is not a major limitation, because geostrophic velocities have weak vertical shears over most of the deep ocean. Snapshots of the bottom velocity every 5 days for a total of 3 years of simulation are used to compute the energy conversion rate.

[16] The skill of the GFDL isopycnal model is addressed in detail by *Hallberg and Gnanadesikan* [2006]. The model surface eddy kinetic energy compares well with estimates from the TOPEX/POSEIDON altimetry. Even though such a comparison does not guarantee any skill for bottom velocities, we are lead to believe that the model is probably reasonably accurate at depth as well because *Scott et al.* [2010] show that four high-resolution models reproduce mean kinetic energy within a factor of two of observations above 3500 m, and within a factor of three below. Additional support for the model skill at depth is shown in Figure 1, where the model bottom velocity and the WOCE stratification are compared against LADCP and CTD data from DP, a region which dominates the global energy conversion as we show below. The data were collected as a part of the "Antarctic Large-Scale Box Analysis and the Role of the Scotia Sea" (ALBATROSS) cruise in March 1999 [*Heywood and Stevens*, 2000]. Taking into account that LADCP data characterize an instantaneous flow field, the bottom velocities are in very good agreement with the data: characteristic bottom speeds in DP are O(10) cm s^{-1} in both model and data. Bottom velocities of O(10) cm s^{-1} are also consistent with current meter observations in DP [*Nowlin et al.*, 1986].

4. Results

[17] Global distributions of topographic roughness, bottom stratification, bottom kinetic energy, steepness parameter, and energy conversion rate are shown in Figure 2. Topographic roughness is computed as an integral of the model spectrum in (5) over the 1 to 10 km wavelength range. Consistent with theories for the formation of abyssal hills [*Goff and Jordan*, 1988], topographic roughness is enhanced along mid-ocean ridges. Regions with the
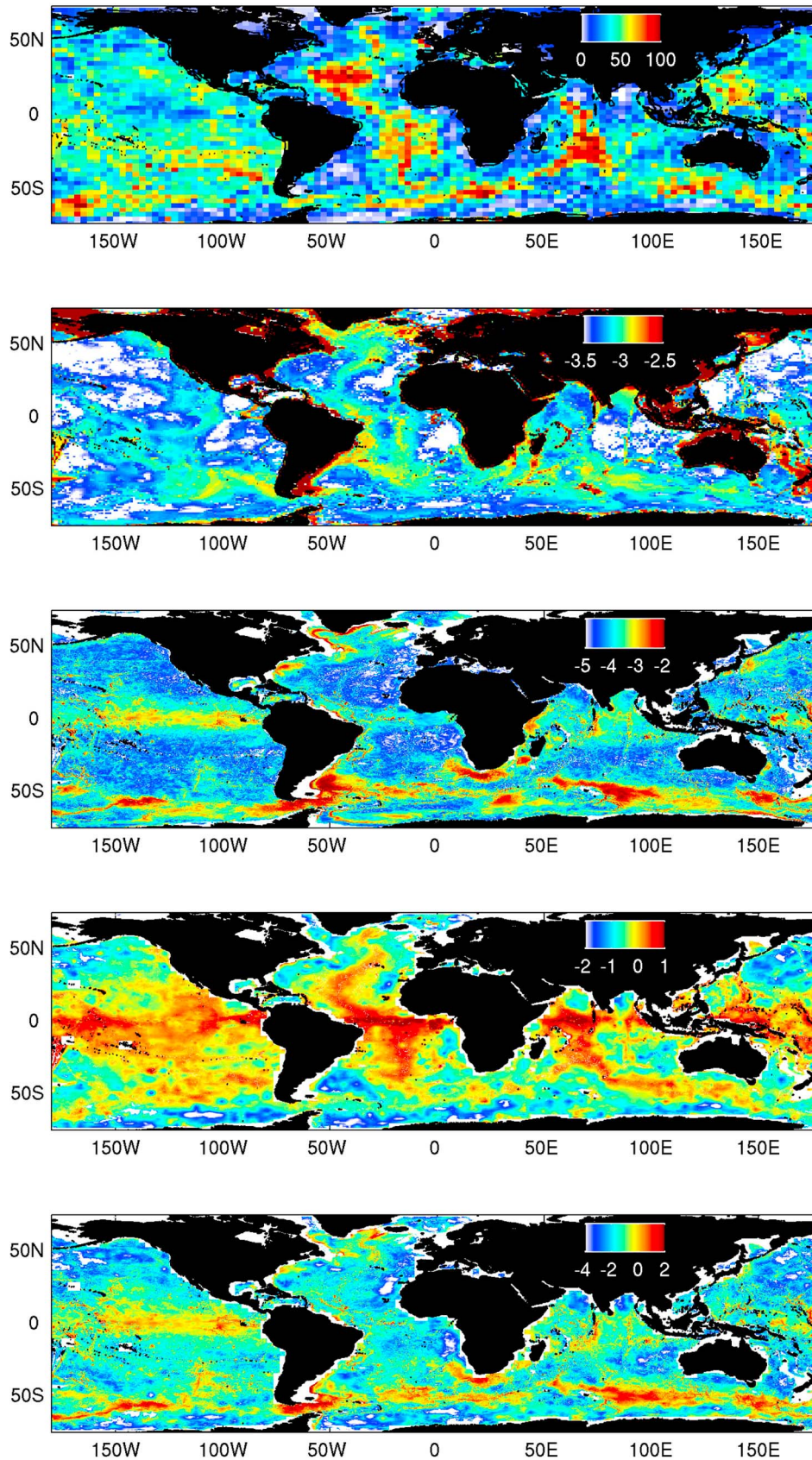
Figure 2. (top) Topographic roughness in (m). (middle top) Bottom stratification in $\log_{10}$ (s^{-1})) estimated using the WOCE hydrographic atlas. (middle) Bottom kinetic energy in $\log_{10}$ ($m^2\ s^{-2}$) obtained from the isopycnal ocean model. (middle bottom) Topographic steepness parameter, $\log_{10} \epsilon$. (bottom) Energy flux into internal lee waves in $\log_{10}$ (mW m^{-2}).

roughest topography at 1–10 km scales are the North Atlantic section of the Mid-Atlantic Ridge (MAR) and the region in the Indian Ocean where three ocean ridges intersect. In the Atlantic Ocean, topographic roughness is enhanced up to 100 m along the MAR and drops to less than 10 m along continental slopes. The Pacific Ocean is characterized by smaller topographic roughness of 40–60 m spread more uniformly throughout the basin. In the SO, topographic roughness is enhanced along the South–West Indian, the South–East Indian, and the Pacific-Antarctic Ridges. The roughness in DP is relatively high, ~60 m, but it does not stand out in the global distribution.

[18] The bottom stratification is enhanced following the mid-ocean ridges because ridges extend a few kilometers up in the water column where stratification is higher. The bottom stratification is $O(10^{-3})$ s^{-1} at mid-ocean ridges where topography is rough, while it is as small as $O(10^{-4})$ s^{-1} over abyssal plains.

[19] The bottom kinetic energy is enhanced in regions of strong currents and high eddy activity such as the SO, western boundary currents, and eastern tropical Pacific. The largest values are found in the SO in regions like DP and in the lee of the Kerguelen Plateau where the bottom kinetic energy reaches up to $O(10^{-2})$ m^2 s^{-2}, corresponding to $O(10^{-1})$ m s^{-1} bottom speeds.

[20] The steepness parameter ϵ varies strongly throughout the ocean with values spanning the sub-critical and super-critical wave radiation regimes. Values of ϵ are supercritical over the mid-ocean ridges where topography is rough and bottom velocity is small: ϵ is inversely proportional to bottom velocity for typical topographic spectral slopes of −2 to −3. Very nonlinear waves are also radiated at the equator where the lee wave frequency is not limited by the Coriolis frequency and waves can radiate from larger topographic features with higher roughness than at mid-latitudes. In the SO, where roughness is smaller and bottom velocity is larger than in ocean basins, values of ϵ are smaller than unity and correspond to sub-critical wave radiation regimes.

[21] The energy conversion rate is enhanced in the SO and the eastern tropical Pacific. The energy conversion reaches up to $O(100)$ mW m^{-2} in regions like DP where high bottom kinetic energy is co-located with elevated topographic roughness. Unlike internal tides [*Nycander*, 2005], lee waves are not radiated over the MAR – the energy conversion is $O(0.1)$ mW m^{-2} – mostly because the bottom eddy kinetic energy is low. The global integral of the energy conversion is 0.2 TW with 0.1 TW taking place in the SO south of 40°S. The global mean of the horizontal and vertical wavelengths of lee waves weighted by the energy flux are 2.5 km and 700 m respectively. Weighted by the energy flux, these scales characterize lee waves radiating energy into the ocean interior away from the bottom boundary layer.

[22] In Figure 1 (bottom), the energy conversion estimate presented in this study is compared against a previous estimate for DP described by NF10b. The previous estimate is based on multibeam topography, LADCP bottom velocity, and CTD-derived bottom stratification data. The energy conversion described here agrees well with the previous estimate:

energy flux in both estimates reaches up to $O(100)$ mW m^{-2} at 59°S, the mean location of the Polar Front of the ACC which dominates the bottom velocity and hence the energy radiation.

[23] To put our results in perspective, the energy conversion from geostrophic flows into lee waves is approximately 20% of the conversion from barotropic to internal tides estimated to be of $O(1)$ TW [*Nycander*, 2005]. The two processes have different geographical distribution. Lee waves are mostly generated in the SO where the energy conversion into internal tides is weak.

5. Summary and Discussion

[24] We applied a linear theory of internal lee wave generation to topographic spectra estimated from single beam soundings, bottom stratification estimated from climatology, and bottom velocity taken from an ocean model. We estimated that 0.2 TW, or 20% of the wind power input, is converted into internal lee waves globally as geostrophic eddies flow over small-scale topography. The energy conversion into lee waves is largest in the SO (~0.1 TW) where bottom geostrophic flows are strong and topography is rough. This estimate does not take into account the presence of a turbulent bottom boundary layer which can reduce the effective roughness of abyssal hills and hence the wave energy radiation. Using idealized numerical simulations with no-slip bottom boundary condition in which a bottom boundary layer develops, NF10a find a 20–30% reduction in energy radiation compared to simulations with free-slip boundary condition and no bottom boundary layer.

[25] Lee waves are characterized by short vertical scales which are highly nonlinear and tend to break close to the generation site. Based on idealized numerical simulations, NF10a and NF10b estimated that up to 50% of the radiated energy is dissipated locally within a kilometer of the topography. Dissipation at a rate of 0.05 TW in the SO can drive a cross-isopycnal flow of $O(10)$ Sv through the bottom kilometer of the water column assuming that the product of the dissipation rate and the mixing efficiency must be equal to the increase of potential energy (see auxiliary material).[1] An $O(10)$ Sv flow is consistent with estimates of the transport of Antarctic Bottom Water [*Ganachaud and Wunsch*, 2000]. That said, it should be clear that the estimates presented here are uncertain and more measurements are needed to better constrain the global budgets.

[27] The Editor thanks two anonymous reviewers for their assistance in evaluating this paper.

References

Adcroft, A., R. Hallberg, J. P. Dunne, B. L. Samuels, J. A. Galt, C. H. Barker, and D. Payton (2010), Simulations of underwater plumes of dissolved oil in the Gulf of Mexico, *Geophys. Res. Lett.*, *37*, L18605, doi:10.1029/2010GL044689.

Arbic, B. K., and G. R. Flierl (2004), Baroclinically unstable geostrophic turbulence in the limit of strong and weak bottom Ekman friction: Application to mid-ocean eddies, *J. Phys. Oceanogr.*, *34*, 2257–2273.

Becker, J. J., and D. T. Sandwell (2008), Global estimates of seafloor slope from single-beam ship soundings, *J. Geophys. Res.*, *113*, C05028, doi:10.1029/2006JC003879.

---

[1]Auxiliary materials are available in the HTML. doi:10.1029/2011GL046576.

Bell, T. H., Jr. (1975), Topographically generated internal waves in the open ocean, *J. Geophys. Res.*, *80*, 320–327.

Ganachaud, A., and C. Wunsch (2000), Improved estimates of global ocean circulation, heat transport and mixing from hydrographic data, *Nature*, *408*, 453–456.

Goff, J. A., and B. K. Arbic (2010), Global prediction of abyssal hill roughness statistics for use in ocean models from digital maps of paleo-spreading rate, paleo-ridge orientation, and sediment thickness, *Ocean Modell.*, *32*, 36–43.

Goff, J. A., and T. H. Jordan (1988), Stochastic modeling of seafloor morphology: Inversion of sea beam data for second-order statistics, *J. Geophys. Res.*, *93*, 13,589–13,608.

Gouretski, V. V., and K. P. Koltermann (2004), WOCE Global hydrographic climatology, *Tech. Rep. 35*, Alfred Wegener Inst., Bremerhaven, Germany.

Hallberg, R. W., and A. Gnanadesikan (2006), The role of eddies in determining the structure and response of the wind-driven Southern Hemisphere overturning: Results from the modeling eddies in the Southern Ocean (MESO) project, *J. Phys. Oceanogr.*, *36*, 2232–2252.

Heywood, K. J., and D. P. Stevens (2000), ALBATROSS cruise report, *Cruise Rep. Ser. 6*, Univ. of East Anglia, Norwich, U. K.

Kunze, E., E. Firing, J. M. Hummon, T. K. Chereskin, and A. M. Thurnherr (2006), Global abyssal mixing inferred from lowered ADCP shear and CTD strain profiles, *J. Phys. Oceanogr.36*, 1553–1576.

Nikurashin, M., and R. Ferrari (2010a), Radiation and dissipation of internal waves generated by geostrophic flows impinging on small-scale topography: Theory, *J. Phys. Oceanogr.*, *40*, 1055–1074.

Nikurashin, M., and R. Ferrari (2010b), Radiation and dissipation of internal waves generated by geostrophic flows impinging on small-scale topography: Application to the Southern Ocean, *J. Phys. Oceanogr.*, *40*, 2025–2042.

Nowlin, W. D., J. S. Bottero, and R. D. Pillsbury (1986), Observations of internal and near-inertial oscillations at Drake Passage, *J. Phys. Oceanogr.*, *16*, 87–108.

Nycander, J. (2005), Generation of internal waves in the deep ocean by tides, *J. Geophys. Res.*, *110*, C10028, doi:10.1029/2004JC002487.

Scott, R. B., B. K. Arbic, E. P. Chassiqnet, A. C. Coward, M. Maltrud, W. J. Merryfield, A. Srinivasan, and A. Varghese (2010), Total kinetic energy in four global eddying ocean circulation models and over 5000 current meter records, *Ocean Modell.*, *32*, 159–169.

Sen, A., R. B. Scott, and B. K. Arbic (2008), Global energy dissipation rate of deep-ocean low-frequency flows by quadratic bottom boundary layer drag: Computations from current-meter data, *Geophys. Res. Lett.*, *35*, L09606, doi:10.1029/2008GL033407.

Wunsch, C. (1998), The work done by the wind on the oceanic general circulation, *J. Phys. Oceanogr.*, *28*, 2331–2339.

Zhai, X., H. Johnson, and D. Marshall (2010), Significant sink of ocean-eddy energy near western boundaries, *Nat. Geosci.*, *3*, 608–612.

R. Ferrari, Department of Earth, Atmospheric and Planetary Sciences, Massachusetts Institute of Technology, Cambridge, MA 02139, USA.

M. Nikurashin, Department of Atmospheric and Oceanic Sciences, Princeton University, Princeton, NJ 08540, USA. (man@alum.mit.edu)